






In-situ loading experiments reveal how the subsurface affects coastal marsh survival

Claudia Zoccarato ^{1,2}, Philip S. J. Minderhoud^{1,3,4}, Paolo Zorzan¹, Luigi Tosi ⁵, Alessandro Bergamasco ⁶, Veronica Girardi¹, Paolo Simonini¹, Chiara Cavallina⁵, Marta Cosma ⁵, Cristina Da Lio⁵, Sandra Donnici⁵ & Pietro Teatini ^{1,2}✉

Over the past decades coastal marshes around the world have declined dramatically. Their deterioration is controlled by scarcity of sediments, erosion and accelerated rise of relative sea-level. The feedbacks between these processes control marsh evolution and determine their long-term survivability. Aggradation of a marsh to keep pace with relative sea-level rise mainly depends on the interplay between sedimentation and autocompaction, but their interactions are severely understudied. Here we present an in-situ loading experiment applied in the Venice Lagoon, Italy, to assess long-term autocompaction, with subsurface displacements and pressure monitored during loading cycles, up to ~40 kN applied on a ~4 m² surface. Two identical experiments carried out in inorganic and organic soil-dominated marshes provided unique insights on the spatio-temporal subsurface dynamics. The large differences in behavior and maximum compaction (6 vs 32 mm) underscore the crucial role of autocompaction and soil heterogeneity when predicting the fate of coastal marshes worldwide.

¹Department of Civil, Environmental, and Architectural Engineering, University of Padova, Padova PD I-35131, Italy. ²Center for Lagoon Hydrodynamics and Morphodynamics, University of Padova, Padova PD I-35131, Italy. ³Soil Geography and Landscape group, Wageningen University, 6708 PB Wageningen, The Netherlands. ⁴Department of Subsurface and Groundwater Systems, Deltares Research Institute, 3584 BK Utrecht, The Netherlands. ⁵Institute of Geosciences and Earth Resources, National Research Council, Padova PD I-35131, Italy. ⁶Institute of Marine Sciences, National Research Council, Venice VE I-30122, Italy. ✉email: pietro.teatini@unipd.it

Coastal marshes are the highest elevated, vegetated landforms within tidal environments. They provide relevant ecosystem functions as carbon sinks^{1,2}, breakers of tidal currents and waves^{3–5}, sediment trapping^{6,7}, buffering of nutrient fluxes from land to the sea^{8,9}, nursery and favorable habitats for a variety of coastal biota, plant and benthic communities¹⁰.

Coastal marshes have declined considerably in area at a global scale over the last decades, with an estimated loss of about 35% between 1970 and 2015^{11,12}. Apart from the unlikely possibility of migrating inland by converting terrestrial uplands to wetlands¹³, long-term survivability of coastal marshes is largely dependent on their capability to gain elevation and keep up with relative sea-level (RSL) rise, thus maintaining their position within the intertidal zone¹⁴. There is wide consensus that vertical accretion of coastal marshes is controlled by physical (e.g., sediment deposition during high tides), biological (e.g., plant productivity), and chemical (e.g., decomposition) processes^{15–18}. Since these processes depend on the relative elevation between the marsh platform and the mean sea-level, they are inherently coupled with the rate of RSL rise¹⁹. Recent coupled biomorpho-geomechanical modeling of long-term marsh evolution highlights how RSL rise is the main factor driving vertical growth in coastal marshes²⁰.

Natural compaction (also referred to as autocompaction) of shallow, recently deposited, unconsolidated sediments, of which the marsh bodies consist of, is one of the components contributing to the total RSL rise. Natural compaction exacerbates the vulnerability of these ecosystems, by reducing elevation gains from accretion. However, after the pioneering works by Cahoon et al.^{21,22} aimed at unraveling compaction and sedimentation from accretion records by means of surface-elevation table (SET) devices, only recently studies started to demonstrate that subsurface processes exert important influence on platform elevation in many wetland systems. Monitoring records of coastal marsh accretion and autocompaction over yearly to decadal periods have been carried out in the Mississippi Delta²³, the Venice Lagoon^{24,25}, and the Ganges-Brahmaputra Delta²⁶ using integrated instrumentation such as SET, feldspar horizons, multiple-depth leveling benchmarks, and persistent scatterer interferometry. Compaction estimates of swamp and marsh sediments (typically mud and peat) over centennial to millennial time-scales have been derived in North Carolina²⁷, Connecticut²⁸, and in the Mississippi Delta²⁹ using geotechnical models empirically calibrated on surface sediments from modern depositional environments analogous to those encountered at depth and on Holocene RSL curves.

However, these approaches are intrinsically characterized by large uncertainties, for example in terms of (i) the loads forcing marsh autocompaction (i.e., what is the actual load exerted by the shallowest few centimeters of soil on the underlying deposits?); (ii) the role played by soil heterogeneity (i.e., how much of the variability in compaction recorded for example in the Mississippi Delta^{23,30} depends on the heterogeneous distribution of the subsoil mechanical properties?); (iii) the nonlinear feedbacks between the various processes driving coastal marsh evolution over mid-to-long time scale. Here, we present a novel in situ loading experiment aimed to characterize the hydro-geomechanical processes governing marsh autocompaction. The experiment was carried out at two marshes located in different depositional environments within the Venice Lagoon, Italy. For the first time, marsh compaction was monitored in undisturbed field conditions under a controlled force of stress (similar to a lab test). The large meter-scale of the experiment suffices to address local lateral and vertical heterogeneities (e.g., those related to plant roots), and enables to simulate long-term natural loading following sediment accretion by a test of few days.

While this experimental approach is challenging to be executed because of the environmental characteristics (e.g., the marshes are

flooded twice a day) and the amount of instrumentation to be transported and established, it offers unique information to anticipate how autocompaction will impact marsh survival in the long term and to evaluate the effectiveness of marsh restoration efforts by means of artificial sediment reintroduction³⁰.

Results

Design of the coastal marsh loading experiment. The presented meter-scale loading experiment, designed following desk studies and preliminary field tests, aims to characterize the hydro-geomechanical response of shallow marsh deposits. The depth interval of interest ranges from surface to 1 m as most autocompaction occurs in this shallow domain³⁰. Autocompaction develops almost exclusively in vertical direction, as horizontal deformation is prevented by symmetrical conditions^{31,32}. Therefore the experiment was designed to resemble a lab oedometer test³³, which is commonly used to characterize vertical soil compressibility while preventing lateral deformation.

The marsh surface is loaded with eight 500-l polyethylene tanks arranged in two rows of four tanks each, filled during loading cycles with seawater pumped from the nearest lagoon creek. The tanks rest on a reinforced geotextile and four wooden pallets to guarantee a uniform load distribution on the marsh surface and eliminate/reduce buoyancy forces on the tanks in high tide conditions (Fig. 1a). The maximum cumulative load, which is reached when all the tanks are filled, amounts to ~40 kN and is distributed on a ~4.0 m² area. The designed configuration allows us to transfer the load on a sufficiently large area, thus i) the assumption of nearly vertical one-dimensional (i.e., oedometer) deformation is acceptable, at least below the central portion of the system, and ii) the response accounts for and averages local-scale heterogeneities of the marsh deposits, for example those due to halophytic vegetation^{16,34}, that cannot be smoothed when few-cm size samples are tested in the lab. Indeed, the experiment is set up on the pristine marsh surface without applying any plants cut off to capture their influence on the soil strength. The field experiment, where the water-filled tanks provide the load, allows us to carry out a compression test at low vertical effective stresses, from 1 to 2 kPa up to a maximum ~10 kPa. Two to four loading and unloading phases, with an increasing percentage of tank filling, are carried out to characterize the marsh soil response in elastic and plastic conditions. By maintaining the load for a sufficiently long time (e.g., more than ~20–24 h in the applications carried out in the Venice Lagoon) the viscous behavior (also called secondary deformation or creep) can be also characterized.

The experiment is equipped with an appropriate monitoring system to measure vertical displacements and groundwater pore-pressure at various depths and locations below the loaded area. The sensors are placed within the ~0.2 m space left from the tank columns (Fig. 1a). In the planned configuration, we use five sensors measuring vertical displacements (Fig. 1a). Three of them are located in correspondence of the load center at the marsh surface (C0) and at 0.1 (C10) and 0.5 m (C50) below the marsh surface, the other two at the edge of the loaded area (E10) and in an intermediate position (M10) at 0.1 m depth. The sensor locations are designed to capture the shape of the soil deformation occurring below the tanks with maximum values occurring at the center of load and decreasing as the edge is approached (Fig. 1b). Moreover, the maximum depth of the sensor (0.5 m below surface) is chosen to capture the main part of the expected deformation. This occurs within a soil depth less than 1 m according to the stress dissipation contours of Fig. 1b. A local benchmark network can be also put in place for an independent check of surface movements during the experiment ongoing.

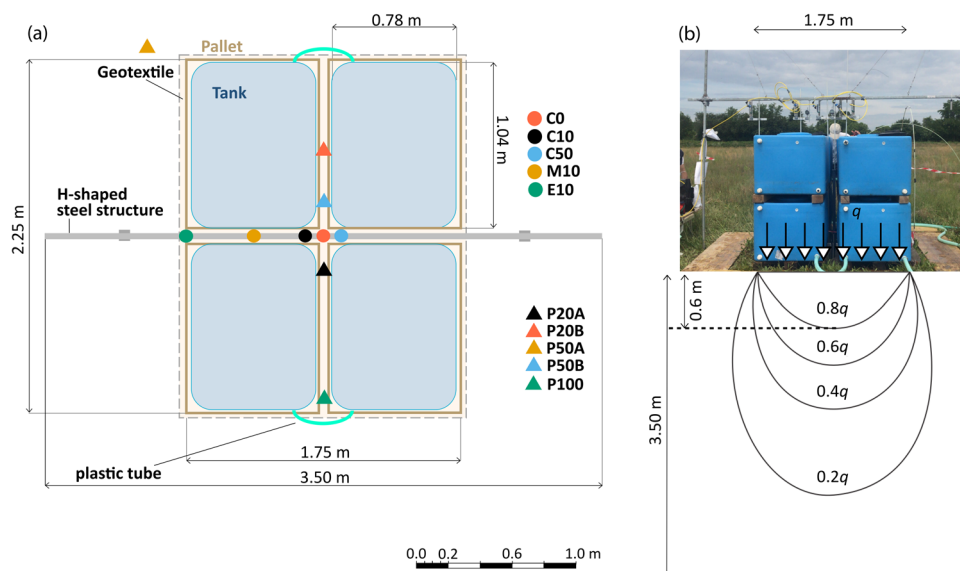


Fig. 1 Design of the loading experiment. **a** Plan view with dimensions, equipment (tanks, pallet, reference steel structure), location of the sensors to measure vertical displacements (bullets) and pore-water pressure (triangles). The sensor coding is representative of the deployment depth (in cm). **b** Qualitative contours of effective stress distribution under a square area loaded by q according to the linear theory of elasticity⁵⁰. In a homogeneous soil the effective stress propagates to a depth twice the square side. The value $80\%q$ propagates to a depth less than one third of the width, that is ~ 0.6 m for the specific case.

Five water-pressure loggers are deployed in the subsurface along the direction orthogonal to the displacement transducers (Fig. 1a) to measure the evolution vs time of the overpressure caused by the surface load. The planned deployment depths are 0.2 (P20A and P20B), 0.5 (P50A and P50B) and 1.0 m (P100). Similarly to displacements, ground-water pressure is measured in correspondence of the load center, at the side of the loaded area and in an intermediate position. Notice in Fig. 1a that a further water-pressure logger must be placed a few meters far from the experimental apparatus to record the pressure behavior caused by natural factors, such as the tidal regime.

The loading experiment was carried out at Lazzaretto Nuovo (LN) and La Grisa (LG) marshes in the northern and southern basin of the Venice Lagoon, respectively (Fig. 2). The elevations of the two marshes at the experimental site are ~ 0.55 (LN) and ~ 0.5 (LG) above msl. Notice that the displacements were logged manually in LN and automatically in LG. More specifications about the experimental set-up and the individual instrumentation employed during the LN and LG tests are reported in Materials and methods.

Displacements and pore-water pressure. The two in situ loading experiments carried out in the Venice Lagoon provide a unique dataset of vertical displacement and pore-water pressure in marsh landforms (Fig. 3). The displacement and pressure values depend on the field site (LN or LG), the depth and location of the deployed sensors, and the (un)loading phase.

At LN, two severe meteorological events (i.e., thunderstorms) occurred in July 2019 interrupting the manual measurements during the experiment and splitting the vertical displacement observations in three disconnected stages. An initial load of ~ 2.8 kPa was applied from 3:00 PM of July 8 and lasted for ~ 5 h (Fig. 3a). The maximum settlement recorded by C10, M10, and E10 amounts to ~ 1 mm, whereas C0 measures 0.4 mm (Fig. 3c). Almost no displacement is recorded by sensor C50. Subsequently, the tanks were emptied and immediately after refilled with a load of ~ 5.6 kPa. The observation interval of 10–15 min implemented during these phases did not allow to record a clear displacement

signal, with the exception of C10 whose displacement reduced from 1.0 to 0.4 mm at the unloading completion and subsequently increased to 2.1 mm at the completion of the second loading phase. Unfortunately, a severe thunderstorm with hail hit the area at 09:20 PM of July 8, soon after the completion of the tank filling, causing a partial destruction of the experimental set-up. The system was rebuilt the day after, resetting the displacement sensors. The ~ 5.6 kPa load was reestablished at 12:30 PM of July 9 and maintained for about 6 h (stage 2). In anticipation of another thunderstorm, the displacement sensors were deinstalled at 18:00 PM out of precaution. The maximum displacements are ~ 1 mm for C0, C10, and M10 and almost zero for C50 and E10. Notice that this phase characterizes the elastic response of the marsh soil since the same ~ 5.6 kPa load was applied the day before. The nearly elastic settlement witnessed during stage 2 was confirmed by the similar (relative) uplift values recorded during the first unloading phase in stage 3 on July 10 (Fig. 3c). After the initial unloading, all eight tanks were fully filled, with the load that peaked at ~ 11.3 kPa after ~ 90 min of filling. This load was sustained for approximately 22 h. A temporary (slight) decrease of load occurred on late July 10 (Fig. 3a) due to high tide, reaching a value of $+0.88$ m above msl (Fig. 3e) and submerging the marsh platform with a water level 0.1 m higher than the tank bottom (Fig. 2c). The maximum settlement amounts to ~ 6 – 7 mm for the most superficial sensors (C0, C10, M10), about 2.5 and 0.7 mm for C50 and E10, respectively (Fig. 3c). Notice the sparse measurements available during the night. The rebound following the final load release is equal to about 3–4 mm for C0, C10 and M10. C50 and E10 show a rebound of 1.6 and 0.4 mm, respectively. The rebound amounts to about 50–60% of the maximum settlement. Optical leveling, using benchmarks unaffected by the thunderstorms, provides a continuous picture of the movements of the marsh landform during the entire loading experiment (Supplementary Fig. 1).

The pore-water pressure observed at LN below the marsh surface is depicted in Fig. 3e together with the tidal water level. After the initiation period of several hours, when water pressure adjusts from atmospheric to field conditions, the behavior measured by each pressure probe is characterized by a plateau.

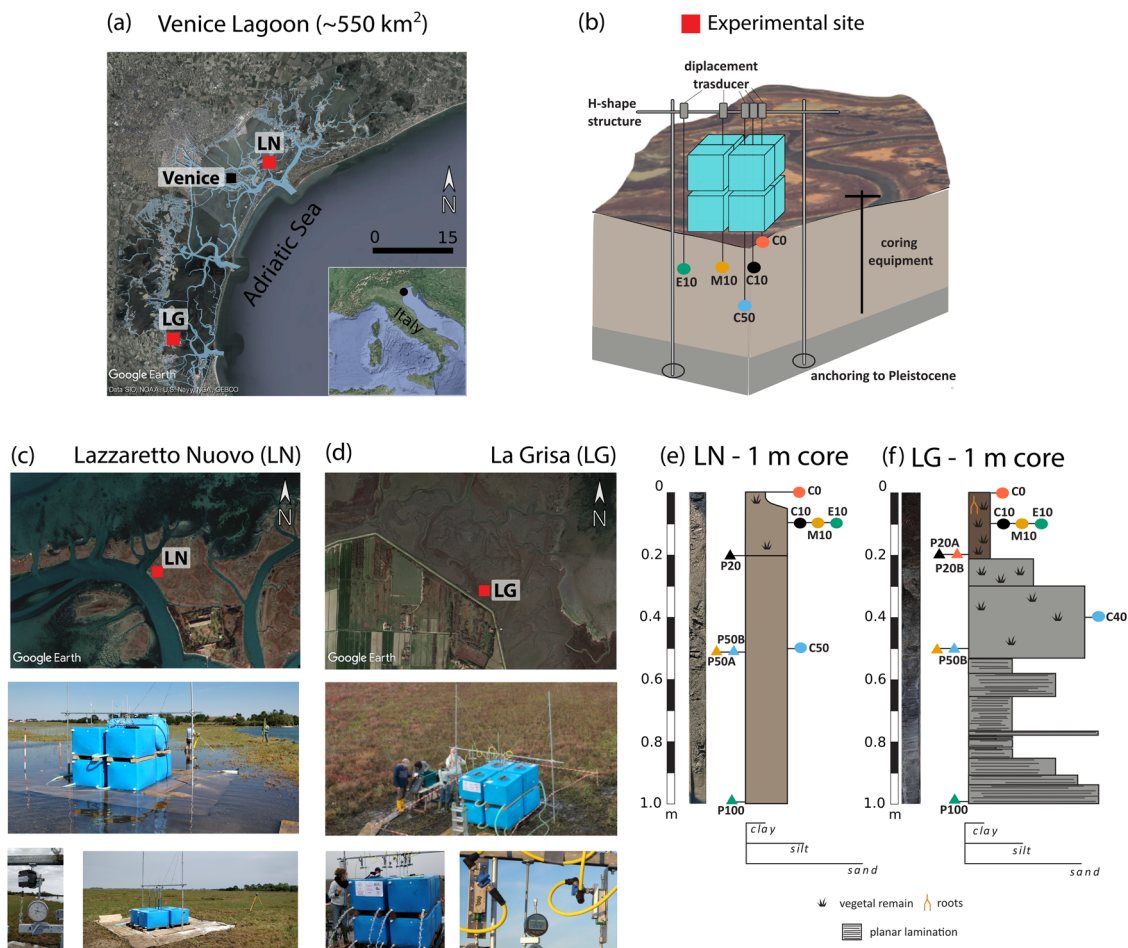


Fig. 2 The loading experiments in the Venice Lagoon (Italy). **a** Map of the Venice Lagoon with the locations of the LN and LG marshes where the loading experiment was carried out in July 2019 and October 2020, respectively. **b** Sketch of the experimental set-up showing the position of the monitoring instruments and the H-shaped structure used as stable reference for the displacement transducers and anchored on the Pleistocene sediments. **c, d** Satellite images of the LN and LG marshes and photos taken during the ongoing experiments. At LN (**c**) the photos show the experimental area loaded with 4 tanks and 8 tanks, in this latter case with the marsh platform submerged during high tide, and a detail of the instruments used to monitor vertical displacements. At LG (**d**) the photos show the experimental area with the 8 tanks (drone photo by Rodrigo Gomila), a detail of the tanks during an emptying (unloading) phase, and the displacement transducers. **e, f** Stratigraphic profiles of the upper 1 m subsoil at LN and LG, respectively. Manual augering equipment was used to characterize the subsurface stratigraphy and collect undisturbed soil samples and cores of the marsh at the two sites in the close vicinity of the loading experiments. The two stratigraphic columns are accomplished with the position of the sensors, which are represented using the same symbols adopted in Fig. 1a.

The values correspond well to the deployment depth and show that the marsh is practically always experiencing saturated conditions. The water pressure has three (or two for P100) major peaks and a number of smaller and shorter (in time) fluctuations. The former are evidently due to the submersion of the marsh platform by seawater during high tides. The latter are caused by the filling/emptying operations of the loading experiment, with pressure that temporarily rises during filling and decreases during emptying. The pressure fluctuations during the (un)loading operations are presented in more detail in Supplementary Fig. 2a. The maximum pore-pressure change range from 0.05 to 0.06 m for P20 to ~ 0.02 m for P100 and vanish shortly after the operation, i.e., in 1 h for P20 and 3–4 h for P100. The above described pore-water pressure fluctuations recorded at various depths contribute to a comprehensive characterization of the marsh body from a hydro-geomechanical points of view. Note for example that the shift of the pore-pressure peaks with respect to forcing factors (tide or experimental operation) increases with depth. Vice versa, the maximum pressure and the speed of pressure decline after the peak decrease with depth. These

behaviors are clearly regulated by the hydraulic conductivity and compressibility of the marsh soil³⁵.

Based on the experience acquired during the LN experiment, a slightly different experimental set-up was implemented in LG, with two loading and two unloading phases that lasted longer to better capture the long-term effect of the prescribed (un)load. Taking advantage of the favorable weather conditions encountered in Fall 2020, we were able to complete the experiment as planned (i.e., the monitoring sensors worked continuously from October 27 to November 2). The first loading phase reached ~ 5.6 kPa (Fig. 3b), i.e., the four bottom tanks were filled, and the load was kept constant over 24 h. The maximum settlement of the marsh surface (sensor C0) equals ~ 10.2 mm (Fig. 3d). C10 and M10 measure ~ 4.4 and ~ 3.4 mm, respectively (approximately 40 and 30% of C0). Settlement at C40 (in LG we were able to reach a maximum 0.4 m deployment depth due to the presence of a stiff silty-sand layer, see Fig. 2f) and E10 amounts to ~ 1.1 and ~ 0.5 mm, respectively (approximately 10 and 5% of C0). The displacement transducers show a clear rebound following the tank emptying operated on October 28 at 4:00 PM. The load

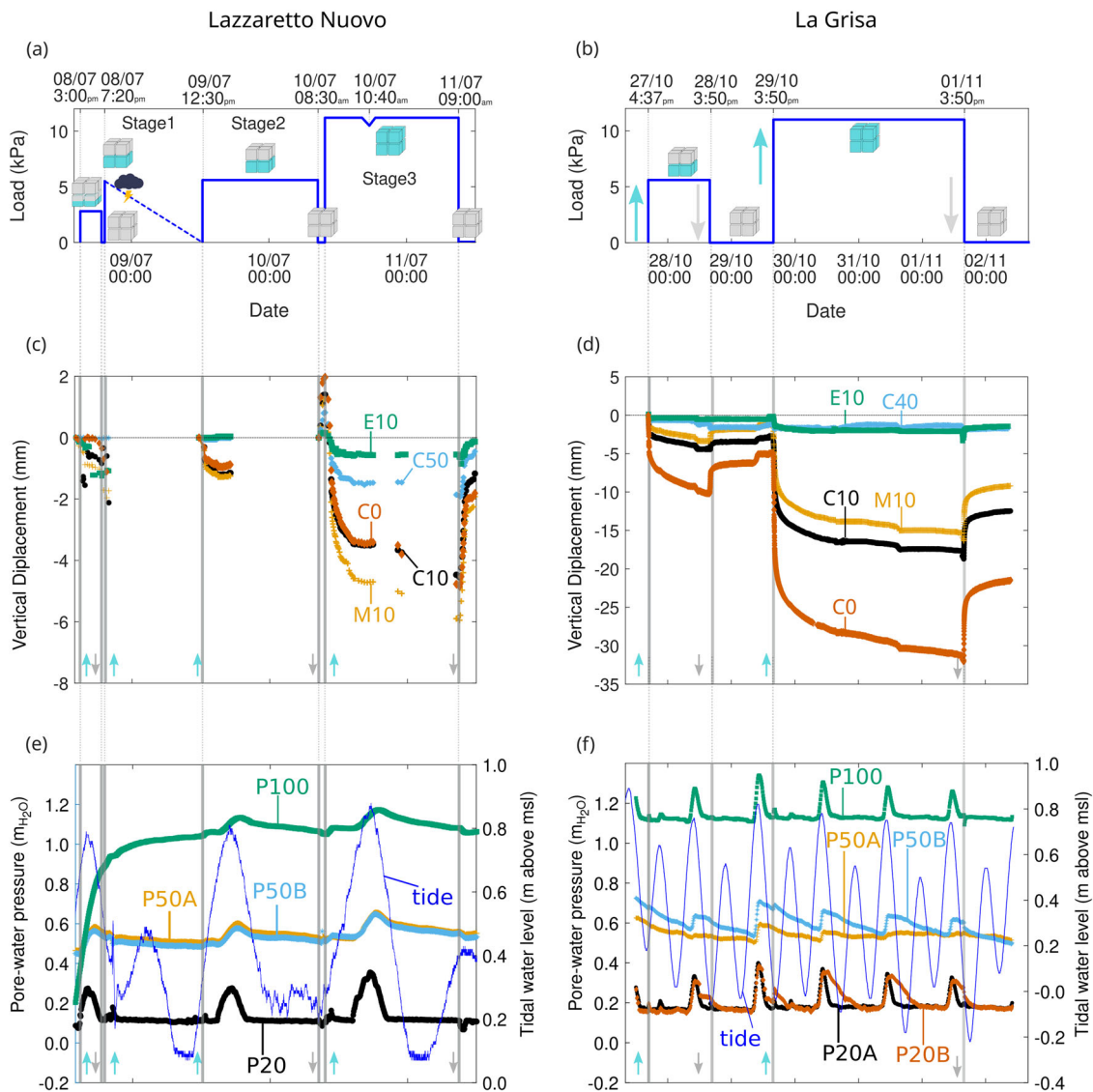


Fig. 3 Datasets collected during the loading experiments at Lazzaretto Nuovo (NL, left panels) and La Grisa (LG, right panels) in the Venice Lagoon.

a, b Load applied on the marsh surface following the various loading and unloading phases with the filling and emptying of the tanks. The filling and emptying last approximately 30–45 min. The loading experiments lasted from July 8 to July 11 in 2019 at LN and from October 27 to November 2 in 2020 at LG. **c, d** Vertical displacement registered by each sensor versus time measured during loading and unloading phases. Negative values mean settlement, positive values mean uplift. C0, C10 and C50 (C40 in LG) are located directly below the load center and refer to the marsh surface, and 0.1 and 0.5 m (0.5 m) depth. E10 and M10 refer to a 0.1 m depth at the edge of the loaded area and in an intermediate position respectively (see also Fig. 1a). **e, f** Pore-water pressure (left axis) and tidal water level (right axis) measured during the loading and unloading phases at various depths. P20, P50, and P100 refer to deployment depth equal to 0.2, 0.5 and 1.0 m below the marsh surface. Letters A and B identify sensors located on the two sides of the experiment, as indicated in Fig. 1a.

remained null for about 24 h. A maximum rebound of ~50%, 40%, 60%, -7%, 67% of the maximum settlement was measured for C0, C10, M10, C40, and E10, respectively.

Consecutively, the load was increased to about ~11.3 kPa and maintained for about 72 h. A further settlement was recorded by all the displacement transducers (Fig. 3d). C0 collects a final settlement of about 32 mm relative to the onset of the experiment. C10 and M10 measure a settlement up to ~18 and ~15 mm. Much smaller are the settlement at C40 and E10, amounting to 1 and 2 mm, respectively. Finally, all eight tanks were emptied and the consequent rebound was recorded for about 24 h. At the end of the experiment, the sensors accumulated a permanent displacement of about 22, 13, 10, 2, and 2 mm for C0, C10, M10, C40 and E10, respectively, corresponding to a settlement equal to ~60–70% for C0, C10, M10 and E10, and ~80% for C40, of the maximum displacement.

The automatic logging of marsh displacements (with a 1 min sampling frequency, much higher than in LN) revealed additional insights in the displacement behavior. Small perturbations were observed in correspondence with the tide peaks, even though the water level on the marsh platform did not reach the tanks, with the exception of that occurred on October 29th at 11:00 AM (0.82 m above msl). Moreover, the curves show clear creep deformation (i.e., secondary, viscous deformation) following the load application after the overpressure dissipation. Notice how the deformation rate (i.e., the slope of the displacement vs time curve) decreases with the monitoring depth.

The behavior of the pore-water pressure for the LG experiment is depicted in Fig. 3f together with the tidal water level fluctuation. They show similar dynamics as seen at LN, e.g., the pore-water pressure followed the tidal level when the marsh was submerged

and the perturbation caused by the (un)loading operations amounts to a few centimeters (up to ~ 0.04 m) and dissipated in about 2–3 h (Supplementary Fig. 2b). However, some peculiarities are worth highlighting: (i) the dissipation of the pore-water pressure after the tide peaks followed the tidal evolution in P20A and P100, but dissipation considerably lagged in P20B, P50A, and P50B; (ii) the sensors deployed at same depth (i.e., P20A and P20B, and P50A and P50B) are characterized by a quite different pressure behavior. The highly heterogeneous lithology distribution (along the vertical direction and, possibly, in horizontal direction as well, Supplementary Fig. 3) is likely responsible of these particular behavior of pore-water pressure evolution.

Environmental, sedimentological and laboratory characterization. Figure 3 shows how LN and LG marshes respond differently to similar loading conditions. To understand their different behavior and correctly interpret the loading experiment outcomes, we combine them with sedimentological and geotechnical investigations with particular focus on the first meter of subsurface.

A number of 1- to 5-m deep cores were sampled along a 200- and 300-m-long transect for the LN and LG salt marshes, respectively. Sedimentological analyses along the transects (Supplementary Fig. 3) revealed the geological evolution of the two sites. The LN salt marsh originally formed on top of a submerged natural levee system supplied by sediments from a lagoon channel connected to a tidal inlet, while the LG marsh developed on top of a mouth bar build by sediments from a former Brenta river mouth that created a delta-like feature inside the lagoon³⁶.

The sedimentological analyses furthermore highlighted the strong vertical and lateral variability characterizing both sites. At LN, the upper 1 m of the deposits consist, from bottom to top, of 0.8 m greyish brown homogeneous silty clay followed by 0.2 m of silty clay, gradually fining upwards to clay with sporadic plant remains (Fig. 2e). The lower homogeneous silty clay layer

represents the deposition of sediments in a tidal flat environment under low energy conditions, while the upper layer, containing plant remains, is associated to the present-day salt marsh environment. The paucity of plant remains and abundance of inorganic sediments reveal that the salt marsh accretion in this area is mainly due to inorganic sediment input, coming from the nearby tidal channel (Fig. 2a).

The 1-m-thick subsoil of the LG experiment site (Fig. 2f), from bottom to top, consists of 0.45 m of laminated very-fine sand to silty clay with a fining upward trend. These latter sediments relate to clastic sediment inputs of the Brenta river when it flowed into the lagoon^{37–39}. Above these deposits, the transition from the deltaic to the lagoonal environment, following the human diversion of the Brenta river away from the site to the sea³⁷, is testified by 0.25 and 0.10 m of silty-sand and silty deposits with plant remains. The uppermost 0.2 m consists of organic clay rich in roots and other plant remains and represents the present salt marsh environment. The abundance of plant remains in the upper layer shows that salt marsh accretion in this area is mainly due to organic matter production, with only little inorganic sediment influx.

In addition to the in situ loading experiment, samples collected at both field sites were subjected to geotechnical laboratory tests. Figure 4 shows the comparison between the field experiments and geotechnical laboratory tests. The latter provided organic matter (based on loss-on-ignition, LOI, tests) and sand percentage (Fig. 4b), and one-dimensional compression curves for samples collected in the upper 1-m depth (see Fig. 4d). For details on the lab methodologies, see Materials and Methods. The full results of laboratory geotechnical investigations are reported in the Supplementary Material in terms of granulometric curves (Supplementary Fig. 4a), hydraulic conductivity (Supplementary Fig. 4b), and one-dimensional oedometric modulus from lab tests (Supplementary Fig. 4c). The sediments at LN are characterized by a high silt fraction and a small sand fraction, showing a slight coarsening in upwards direction (Supplementary Fig. 4a). The organic matter content varies from 10 to 15% in the upper 0.2 m, and reduces to

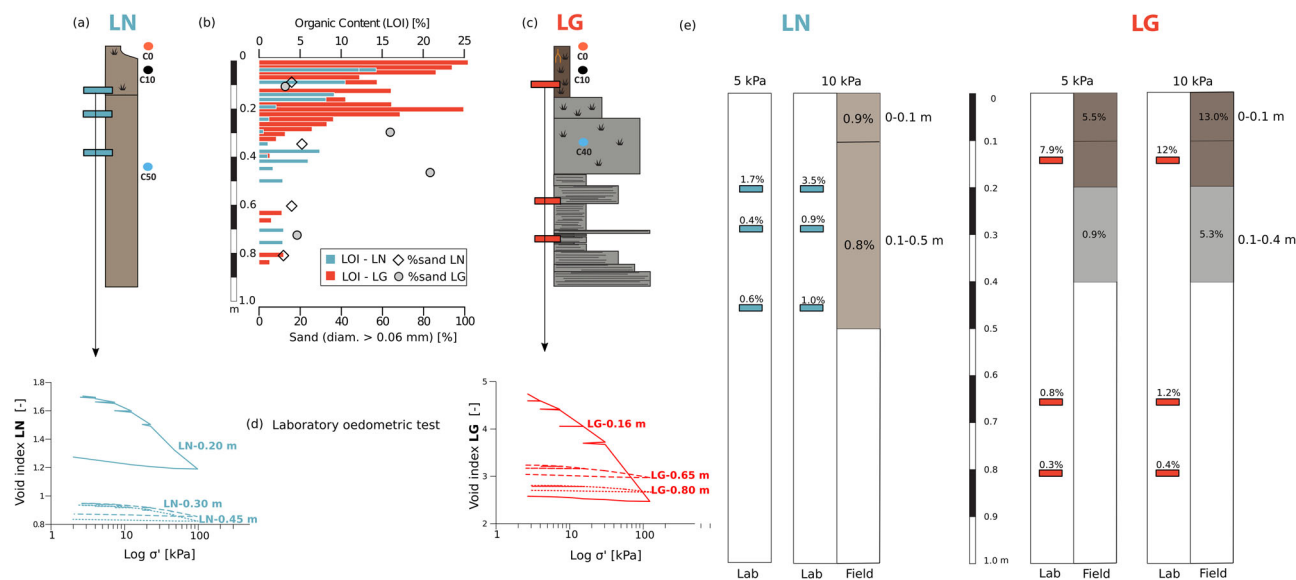


Fig. 4 Comparison between field measurements and geotechnical laboratory test results for Lazzaretto Nuovo (LN) and La Grisa (LG). **a, c** Position of the displacement transducers and oedometer samples in the 1-m stratigraphic profiles of Fig. 2e, f. **b** Organic content obtained through LOI tests and sand percentage derived from the granulometric curves (Supplementary Fig. 4a). The sand percentage allows us to easily recognize the stiff layer between 0.3 and 0.5 m where the C40 sensor was positioned at LG. **d** Results of the classical oedometric tests (void index versus effective stress). Undisturbed samples were collected at 0.2, 0.3 and 0.45 m at LN (Fig. 4a) and 0.16, 0.65 and 0.80 m at LG (Fig. 4c). **e** Comparison of field and lab deformations at ~ 5 and ~ 10 kPa. Field data provide an average value over the depth intervals between 0.0 and 0.1 m depth and from 0.1 to 0.5 m (0.4 m at LG) depth, while lab data provides point estimates at the respective sample depths.

few percent at larger depth (Supplementary Fig. 4b). Oedometric tests were performed on samples at 0.2, 0.3 and 0.45 m depth and provide values for the compression index, C_c , and the recompression index, C_r . The C_c , i.e., the slope of the virgin compression line, is equal to 0.4 at 0.2 m depth and ~ 0.1 at 0.3 and 0.45 m depth. The C_r , i.e., the slope of the reloading part of the curve, amounts to 0.043, 0.002 and 0.006 at 0.20, 0.30 and 0.45 m depths, respectively (Fig. 4d). Permeability tests were performed during the 1D compression, providing a hydraulic conductivity ranging between 7×10^{-9} and $2 \times 10^{-8} \text{ m s}^{-1}$ at a stress level of 20 kPa (Supplementary Fig. 4b). This value is coherent with the silty nature of these soils. At LG, the granulometric distribution shows a strong dominance of sand in the central portion of the soil, i.e., between 0.2 and 0.6 m, reaching values in the range 60–85% (Fig. 4b). In the shallower and deeper parts, the silt fraction is dominant and sand percentages drop to the range 12–20% (Supplementary Fig. 4a). LOI is particularly high in the shallow part, in the first 0.2 m averaging 20% with peaks of 25% (Fig. 4b), agreeing well with the abundance of plant remains in the top portion of the analyzed sequence. Below this depth, LOI rapidly decreases to $\sim 3\%$, with values similar to those quantified at LN. Oedometric tests were performed on samples at 0.16, 0.65 and 0.8 m depth (Fig. 4d). The C_c is ~ 0.2 at 0.65 and 0.8 m depth. C_c could not be computed at 0.16 m due to a non-distinguishable single slope of the void index - effective stress curve. The C_r values amount to 0.07 and 0.01 at 0.16 and 0.65 m depth, respectively. At 0.8 m depth C_r assumes a negative value, which is non-physical. The hydraulic conductivity varies with depth from $5 \times 10^{-10} \text{ m s}^{-1}$ at 0.16 m to $\sim 10^{-8} \text{ m s}^{-1}$ at 0.65 m and $\sim 8 \cdot 10^{-9} \text{ m s}^{-1}$ at 0.8 m (Supplementary Fig. 4b). Notice that this parameter is not largely influenced by the effective stress in the range from 3 to 20 kPa. The smallest hydraulic conductivity corresponds to the shallowest soils, coherently with the clayey nature of these layers, while the higher values in the mid-depth levels are in agreement with a high percentage of sand (Fig. 4b).

The oedometric or tangent modulus M (Supplementary Fig. 4c), representing the soil stiffness, usually varies with stress (or load). For the shallowest (0.20 m) and deepest (0.45 m) samples at LN, M ranges from 0.26 to 1.05 MPa and between 1.36 and 2.60 MPa, respectively. At LG, M varies from 0.05 to 0.87 MPa and between 2.27 and 9.14 MPa for 0.16 and 0.80 m depth, respectively. The testing stress ranged from ~ 3 and ~ 100 kPa.

Discussion and implications

One of the main determining factors for coastal marsh survival under RSL rise is their ability to carry the load exerted on their surface by new (natural or artificial) sediments^{25,30,40}. Evidence from the field⁴¹ and model computations⁴² suggested that this is not a given thing. Our results demonstrate that, within the same coastal system, autocompaction can spatially be highly variable and largely depends on the characteristics of the soil that composes the marsh landform, i.e., on the specific depositional environments where a marsh grows and thickens.

The stratigraphic analyses carried out in the two marshes in the Venice Lagoon reveal that deposition of inorganic sediments is dominant at LN, whereas organic production is primarily responsible for accretion of the LG marsh. These observations are consistent with the present geomorphological characteristics of the two sites. The LG site is located in the inner margin of the lagoon, far from direct sources of inorganic sediments⁴³, whereas the LN site is located at the edge of a tidal channel near the Lido inlet, where inorganic sedimentary input is abundant. Based on these considerations and the outcome of the loading experiments

we can anticipate that surface-elevation change with a similar amount of accretion can strongly differ between LN and LG marshes, with a ratio of 5 to 1. Oedometric laboratory experiments with samples collected from marshes around the world with similar geologic settings (Table 1) confirms that organogenic marshes (high LOI values) are always positively correlated with compression indices and void ratios, leading to higher consolidation rates compared to minerogenic marshes. LOI values in the range 30–50% leads to $C_c \sim 2$ –4 and $C_r \sim 0.1$ –0.5. Low LOI percentages drop the indices to $C_c \sim 0.02$ –0.2 and $C_r \sim 0.002$ –0.1, respectively. LOI is also correlated with preconsolidation stress σ_p , where more organic content reflects lower σ_p values and a higher tendency to consolidate. However, we stress that the in situ experiment supplies different information on geomechanical properties compared to lab data, providing average estimates over decimeter depth intervals instead of point estimates at sample depths.

These findings question the reliability of recent model prediction of the long-term response of coastal wetlands to future RSL rise, at specific locations⁴⁴ or globally¹³, as they neglect the role played by autocompaction and/or the inherent heterogeneous nature of the marsh subsurface. Indeed, high variability rates of shallow subsidence are available for several coastal marshlands and deltaic areas worldwide (Table 2). For example, shallow subsidence at San Felice marsh (Table 2), a silty-sand marsh located nearby the LN site, shows rates in the range of 0.0–2.0 mm year⁻¹. Rates of few mm/year are also reported by other authors^{21,45,46}. However, in different subsurface setting, rates might be ten times higher with values up to ~ 50 mm year⁻¹^{47,48}. Note that measurements refer to different sediment thicknesses. A comparison with SLR values measured by remote sensing in front of this areas shows that shallow subsidence and SLR are generally comparable with some exceptions where SLR is about five times higher than subsidence⁴⁵ or, conversely, subsidence is one order of magnitude larger than SLR^{47,48}.

Properly accounting for autocompaction will provide reliable quantifications of deposition rates required for a marsh to keep pace with RSL rise, including the consideration that autocompaction varies following the lithological characteristics of both the existing marsh soil and the new deposits. Moreover, the need to couple surface and subsurface processes in high-resolution, physics-based numerical modeling of coastal marsh evolution has been recently pointed out^{19,20,49}.

The results from the in situ loading experiments provide new insights that progress our understanding of the hydro-geomechanical behavior of coastal marshes, likely valid for similar landforms worldwide. Firstly, cross-comparison of results from laboratory tests and the loading experiments in the field (Fig. 4e) allows us to evaluate the pros and cons of the in situ testing approach. Displacements recorded in the marshes at the center of the loading area were converted to deformation (Fig. 4e) and validated against values obtained in the lab from oedometric tests (Fig. 4d). We can compare two loading stages (at LN only one due to the instrumentation problems caused by the thunderstorm), i.e., four and eight tanks filled by seawater, respectively amounting to ~ 5.6 and ~ 11.3 kPa, and two depth intervals, between the marsh surface and 0.1 m and from 0.1 to 0.5 m (0.4 m at LG) depth using records provided by sensors C0, C10, and C50 (C40 at LG). At LN, field deformation averages 0.9% in the shallow and 0.8% for the deep interval. Deformation measured in the lab under similar loading conditions ranged from 0.4 to 1.7% and 0.9 to 3.5% for 5.6 and 11.3 kPa. These data refer to samples collected at 0.2 and 0.45 m depth, i.e., the layer between sensors C10 and C50 (Fig. 4e). At LG field deformations of the top 0.1-m interval were 5.5% and 13% for the half and full load, respectively. The values decreased respectively to 0.9% and

Table 1 Geotechnical characterization of marshes around the world by oedometric laboratory tests.

Study site	Sediment depth (m)	Geotechnical parameters				Reference		
		LOI (%)	G _s	e ₀ (1) or e _t (2)	C _c		C _r	σ _p (kPa)
Cowpen Marsh, UK	0.2	5-40	2.25-2.60	1-10 (2)	0.18-2.96	0.009-0.38	3-17	Brain et al. (2012) ⁴⁵
Roudsea Marshland, UK	0.2	2-15	2.56-2.68	1-3 (2)	0.09-0.97	0.005-0.10	3-10	
Thornham Marsh, UK	0.2	1-30	2.38-2.66	0.76-6 (1)	0.02-2.17	0.002-0.08	7-16	
Tillingham Marsh, Essex, UK	0-0.6	Clay/silt-dominated		1.82-2.77	0.66-1.0 ^a	0.12 ^a	18-27	Brooks et al. (2022) ⁶⁶
Warton Marsh, Morecambe Bay, UK	0-0.6	Sand/silt-dominated		0.98-1.15	0.04-0.37 ^a	0.05 ^a	23-65	
East River Marsh, Connecticut, USA	0.15	9-40	2.11-2.53	2.38-8.8 (2)	0.63-4.12	0.02-0.15	4-8	Brain et al. (2017) ²⁸
Tump Point, North Carolina, USA	0.15	30-50	2.05-2.22	7.26-10.75 (2)	3.09-4.02	0.10-0.48	3.5-4.5	Brain et al. (2015) ²⁷
Lazzaretto Nuovo Marsh, Venice, Italy	0.2-0.5	1-15	2.6-2.78	0.99-1.77 (1)	0.1-0.4	0.002-0.04	18-19	This study (lab test)
La Grisa Marsh, Venice, Italy	0.6-0.9	1-3	2.7-2.8	1.76-2.81 (1)	0.17-0.26	0.01	8-24	Cola et al. (2008) ⁶⁷
San Felice Marsh, Venice, Italy	0.1-0.6	2-7	2.7	0.81-1.28 (1)	0.14-0.24	0.025-0.033	20-40	
Rigà Marsh, Venice, Italy	0.1-0.6	2-13	2.7	2-5 (1)	0.1-1.4	0.003-0.3	10-50	
Shallow marsh deposits, Mekong delta, Vietnam ^b	0-20	Up to 10	2.59-2.71	1.47-2.29 (1)	0.52-0.97	0.09-0.21	-	Toan and Nu (2013) ⁶⁸
Buried paleomorph, Mekong delta, Vietnam ^b	28.05-38.9	8	-	-	0.6-0.83	0.06-0.09	13-215	Hoang et al. (2016) ⁶⁹
Big River, Hynes Brook, Placentia - Newfoundland, Canada	Surface sediments	12-80	1.98-2.75	3-16 (2)	0.8-4.0	0.02-0.32	3-12	Kemp et al. (2018) ⁷⁰

At each study site, the table reports minimum and maximum values of loss-on-ignition (LOI), specific gravity (G_s), initial void ratio (e₀) or void ratio at 1 kPa (e_t), compression and recompression indices (C_c and C_r), and preconsolidation stress (σ_p) obtained by samples collected at the specified depth.
^aValues calculated from data published in the specified reference.
^bAverage values from selected sites throughout the Mekong delta.

5.3% in the deeper interval (0.1-0.4 m). Oedometric lab tests provide 7.9% and 12% at 0.16 m, 0.8% and 1.8% at 0.65 m, 0.3% and 0.4% at 0.8 m depth for 5.6 and 11.3 kPa, respectively (Fig. 4e). The general consistency between field and lab quantifications demonstrates that the loading test design ensures the validity of the oedometric assumption, i.e., vertical deformation with precluded lateral expansion. This is important because the uniaxial vertical compressibility controls the long-term evolution of marsh elevation, playing a key role for survival or drowning of coastal marshes²⁰. Notice that classical geotechnical solutions⁵⁰ do not represent the behavior of these landforms well. At LN the ratio (displacement_{C0}) over (displacement_{C50}) amounts to ~2.4, and at LG (displacement_{C0}) over (displacement_{C40}) is equal to ~15. These values are far from the value ~1.2 that you might expect from Fig. 1b, especially at LG where the soil is characterized by a large vertical heterogeneity in sediments.

A second interesting outcome is related to marsh behavior during the unloading phase when the water tanks were being emptied. Soil is more deformable during loading than during unloading, as only part of the deformation is reversible. The ratio *s* of compressibility during loading (i.e., partially irreversible deformation) and unloading (i.e., only reversible deformation) is reported to decrease with depth⁵¹ from *s* = 20 – 100 at depth less than 100 m down to *s* = 1.5 – 3 in deep reservoirs. Tests carried out at the Treporti littoral strip of the Venice Lagoon^{52,53} to support the design of the MoSE mobile gates⁵⁴ at lagoon inlets revealed that compressibility of shallow soils in unloading condition is ~15 times smaller than in the loading phase^{55,56}.

Our results achieved by the LN and LG experiments are surprising in this respect as they provide *s* ~2 only (Fig. 3c, d). Such a highly recoverable response of the shallowest marsh soil is unexpected, also compared with the C_c and C_r values provided by the lab oedometric tests carried out on the samples collected in the two sites (Fig. 4d) suggesting *s* ~10. We believe that this effect is mainly associated to the presence of the in situ root structure of the living vegetation cover present in the upper 0.20–0.25 m. This is in agreement with recent reports on the beneficial effects exerted by halophytes roots and rhizomes on marsh shear and compressibility strength^{18,57}.

For the first time to our knowledge, creep behavior was witnessed and measured in marsh soils. Creep is the long-term viscous deformation caused by rearrangement of the sediment skeleton by the force of gravity under constant effective stress⁵⁸. Notice that we refer here to a different process than the creep investigated by Mariotti et al.⁵⁹, where the term is used to describe movements of sediments along channel bank slopes causing lateral marsh erosion. Creep is generally associated to loading of soft fine sediments with large structures⁶⁰. It develops as secondary compression, after the dissipation of pore overpressure (causing primary compression) following an increase in loading. In a marsh under natural conditions loading is caused by sediment accretion. However, as sedimentation develops continuously and slowly over time, (primary) compaction and creep have never been distinguished in marsh autocompaction before. The application of a constant load over a time interval much longer (i.e., days) than that required to dissipate the tank filling-related overpressure (i.e., hours) (Fig. 2), allows us to disentangle creep from the cumulative deformation and quantify the creep coefficient C_α, which is the slope of the curve vertical deformation vs log time. Referring to LG, we compute C_α = 2.5 × 10⁻² and C_α = 1.3 × 10⁻² for the shallow (surface to 0.1 m) and deeper depth intervals (0.1-0.4 m), respectively (Fig. 3d). Interpretation of the displacement records at the trial embankment in Treporti⁶¹ provided C_α = 10⁻³ – 4 × 10⁻³, one order of magnitude less than the values from the loading experiment.

Table 2 Comparison of shallow subsidence and SLR in coastal environments worldwide.

Study site	Shallow subsidence (mm/year)	Sediment thickness (m)	Measured (M) or computed (C)	SLR ^a -SLR ^b (mm/year)	Reference
San Felice marsh, Venice, Italy	0.0-2.0	5	M	1.2-2.9	Da Lio et al. (2018) ²⁴
Novissimo marsh, Venice, Italy	1.0	5	M	1.2-2.9	
Synthetic succession with measured geotechnical values	0.1-0.4	1-3	C	1.1-2.5	Brain et al. (2012) ⁴⁵
Bayou Chitigue, Mississippi delta plain, USA	24.5	4	M	1.0-3.3	Cahoon et al. (1995) ²¹
Old Oyster Bayou, Mississippi delta plain, USA	3.9	4	M	1.0-3.3	
St. Marks NWR, Florida, USA	5.2	3	M	1.0-3.3	
Cedar Island NWR, North Carolina, USA	2.3	5	M	1.2-2.1	
Mississippi delta, USA	7.1	20	M	1.0-3.3	Jankowski et al. (2017) ²³
Barrier Island in the North Sea	1.0	45	C	1.1-4.2	Schuerch et al. (2012) ⁴⁶
Mekong Delta, Vietnam	13.4-49.5	10-22	M	1.2-4.2	Giao et al. (2014) ⁴⁷ ; Lovelock et al. (2015) ⁴⁸
Ganges-Brahmaputra lower plain delta, Stream-Bank	11.3	15-20	M	1.0-3.8	Bomer et al. (2020) ²⁶
Ganges-Brahmaputra lower plain delta, Interior	8.0	15-20	M	1.0-3.8	
Cumberland Marshes, Canada	15.0	8	C	0.0-1.6	van Asselen et al. (2011) ⁷¹
Peatlands in the Rhine-Meuse delta, The Netherlands	0.6	3-5	C	1.1-2.5	van Asselen et al. (2011) ⁷²

At each study site the table reports the thickness of the sediments considered to measure or compute the subsidence and values of regional sea-level trends based on measurements from satellite altimeters. ^aValues of SLR taken between 1992 and 2014 based on data collected from the TOPEX/Poseidon, Jason-1 and Jason-2 satellites (after NASA's Scientific Visualization Studio. <https://svs.gsfc.nasa.gov/4345>). ^bValues of SLR taken between 1992 and 2018 (courtesy of CNES/LEGOS/CLS/EU Copernicus Marine Service/contains modified Copernicus Sentinel data, 2018. https://www.esa.int/Applications/Observing_Earth/Spotlight_on_sea-level_rise).

Long-term projections of coastal marsh resilience to RSL rise should not neglect the importance of subsurface processes and the effects of autocompaction. To do so, the complex interactions of processes happening at the surface and within the subsurface of a marsh need to be recognized and quantified. The novel in situ loading experiment presented here is a promising cost-effective methodology to characterize the hydro-geomechanical properties of marsh soils. It can be viewed as an anticipation of the long-term natural autocompaction, squeezed in a test of several days.

Materials and methods

Set-up of the field experiments in the Venice Lagoon. The execution of the loading experiment in the marshes of the Venice Lagoon was challenging from several points of view. The marshes are difficult to reach, the material transportation is not easy, the setting up of the specific instrumentation required to track the evolution of the hydro-geomechanical parameters is not straightforward without disturbing the marsh soil, thus affecting the potential test results. In addition, the marshes are flooded twice a day during high tides.

The tank dimensions we used are $0.78 \times 0.69 \times 1.04 \text{ m}^3$. Each tank can contain up to 500 l and its empty weight is approximately 0.1 kN. The tanks were placed with a 0.1–0.2 m gap between them, allowing for an optimal positioning of the monitoring instrumentation. Consequently, the whole loading area became $2.25 \times 1.75 \text{ m}^2$. The tanks were interconnected at the bottom through plastic tubes to guarantee the same water levels during filling and, consequently, a uniform distribution of the load (Fig. 1).

The five displacement transducers installed to measure marsh compaction were attached at one end to a H-shaped steel structure anchored on two steel piles with a foundation at ~6 m depth where an over-consolidated layer was located. The other end was fixed to the prescribed soil depth (i.e., from the surface to 0.5 m) through an aluminum anchor specifically designed to account for two main constraints: (i) minimize the disturbance to the soil during the insertion of the anchor to its reference depth; and (ii) guarantee that it remains anchored to the depth of interest given the loose nature of the shallow marsh deposits. The anchor was constituted by a 0.05 m radius helicoidal disk with a 0.5 m long and 0.005 m diameter wire in the center. The anchor was inserted into the soil by rotational force only with no vertical force.

The displacements of the reference H-shaped steel structure and the four external corners of wooden pallets carrying the tanks were monitored during the whole test by means of very-high precision spirit leveling. A reference benchmark was established 50 m far from the load using a steel pole inserted into the soil at about 6 m depth. The tidal water level was measured in the channel in front of the experiment and the gauge equipment was also reference to the benchmark.

A wooden boardwalk was placed around the experiment on the marsh surface to minimize disturbance of the marsh and loading induced by the people during the construction and duration of the experiment.

Monitoring equipment

Lab characterization—grain size, compressibility and hydraulic conductivity. Grain size analyses were carried out in a conventional manner using sieves for the particles ranging from 0.075 to 100 mm, and the hydrometer method for the particles smaller than 0.075 mm. The procedure for the sieve grain size analysis was based on the standard ASTM D6913 while the use of the hydrometer method was based on the standard ASTM D7928^{62,63}. Loss-on-ignition was measured by comparing weight measures of a soil sample before and after introducing the sample in an oven at 440 °C for 33 h. The procedure follows the standard of ASTM D7348⁶⁴. Oedometer tests were performed with a conventional apparatus, considering samples of 2 cm thickness by 5–7 cm diameter. The load sequence and entity were specifically designed accordingly to the typical loads acting on a marshland: tidal loads, inducing cycles of load and unloads of few kPa on the shallow portion of the marshland; but also processes of sedimentation and erosion. During the test, the sample was fully saturated, with top and bottom drainage ensuring the excess pore-pressure dissipation during each load step. The deformation of the sample was continuously monitored with a LVDT sensor. In this manner it was possible to retrieve the deformation history associated to the loads/unloads applied, compressibility coefficients, preconsolidation pressure and preconsolidation stress. The determination of permeability coefficients was carried out during the oedometer tests at different stress levels. Accordingly to the fine texture of the soils, the falling head technique was used to evaluate the permeability coefficients.

Data availability

Source information from the figures can be found at <https://doi.org/10.25430/RESEARCHDATA.CAB.UNIPD.IT.0000071565>.

Received: 1 April 2022; Accepted: 19 October 2022;

Published online: 03 November 2022

References

- Mcleod, E. et al. A blueprint for blue carbon: toward an improved understanding of the role of vegetated coastal habitats in sequestering CO₂. *Front. Ecol. Environ.* **9**, 552–560 (2011).
- Were, D., Kansime, F., Fetahi, T., Cooper, A. & Jjuuko, C. Carbon sequestration by wetlands: a critical review of enhancement measures for climate change mitigation. *Earth Syst. Environ.* **3**, 327–340 (2019).
- Duarte, C., Losada, I., Hendriks, I., Mazarrasa, I. & Marbà, N. The role of coastal plant communities for climate change mitigation and adaptation. *Nat. Clim. Change* **3**, 961–968 (2013).
- Möller, I. et al. Wave attenuation over coastal salt marshes under storm surge conditions. *Nat. Clim. Change* **7**, 727–731 (2014).
- Van Coppenolle, R., Schwarz, C. & Temmerman, S. Contribution of mangroves and salt marshes to nature-based mitigation of coastal flood risks in major deltas of the World. *Estuar. Coasts* **41**, 1699–1711 (2018).
- Li, H. & Yang, S. L. Trapping effect of tidal marsh vegetation on suspended sediment, Yangtze Delta. *J. Coastal Res.* **25**, 915–930 (2009).
- Donatelli, C. et al. A nonlinear relationship between marsh size and sediment trapping capacity compromises salt marshes' stability. *Geology* **48**, 966–970 (2020).
- Dame, R. F. et al. Annual material processing by a salt marsh-estuarine basin in South Carolina, USA. *Mar. Ecol. Prog. Ser.* **72**, 153–166 (1991).
- Bonometto, A. et al. Factors controlling sediment and nutrient fluxes in a small microtidal salt marsh within the Venice Lagoon. *Sci. Total Environ.* **650**, 1832–1845 (2019).
- Whitcraft, C. & Levin, L. Regulation of benthic algal and animal communities by salt marsh plants: Impact of shading. *Ecology* **88**, 904–917 (2007).
- Davidson, N. C. & Finlayson, C. M. Extent, regional distribution and changes in area of different classes of wetland. *Mar. Freshw. Res.* **69**, 1525–1533 (2018).
- Global Wetland Outlook: State of the World's Wetlands and their Services to People. Tech. Rep., Ramsar Convention on Wetlands. Gland, Switzerland: Ramsar Convention Secretariat (2018).
- Schuerch, M. et al. Future response of global coastal wetlands to sea-level rise. *Nature* **561**, 231–234 (2018).
- Kirwan, M. et al. Limits on the adaptability of coastal marshes to rising sea level. *Geophys. Res. Lett.* **37**, L23401 (2010).
- Kirwan, M. & Megonigal, P. Tidal wetland stability in the face of human impacts and sea-level rise. *Nature* **504**, 53–60 (2013).
- Marani, M., Da Lio, C. & D'Alpaos, A. Vegetation engineers marsh morphology through multiple competing stable states. *Proc. Natl. Acad. Sci. USA* **110**, 3259–3263 (2013).
- Morris, J. T., Sundareshwar, P. V., Nietch, C. T., Kjerfve, B. & Cahoon, D. R. Response of coastal wetlands to rising sea level. *Ecology* **83**, 2869–2877 (2002).
- Cahoon, D. R., McKee, K. L. & Morris, J. T. How plants influence resilience of salt marsh and mangrove wetlands to sea-level rise. *Estuar. Coasts* **44**, 883–898 (2021).
- Fagherazzi, S. et al. Salt marsh dynamics in a period of accelerated sea level rise. *J. Geophys. Res. Earth Surf.* **125**, e2019F005200 (2020).
- Zoccarato, C., Da Lio, C., Tosi, L. & Teatini, P. A coupled biomorpho-geomechanical model of tidal marsh evolution. *Water Resour. Res.* **55**, 8330–8349 (2019).
- Cahoon, D. R., Reed, D. J. & Day, J. W. Estimating shallow subsidence in microtidal salt marshes of the southeastern United States: Kaye and Barghoorn revisited. *Mar. Geol.* **128**, 1–9 (1995).
- Cahoon, D. R. et al. High-precision measurements of wetland sediment elevation: II. The rod surface elevation table. *J. Sediment. Res.* **72**, 734–739 (2002).
- Jankowski, K. L., Törnqvist, T. E. & Fernandes, A. M. Vulnerability of Louisiana's coastal wetlands to present-day rates of relative sea-level rise. *Nat. Commun.* **8**, 14792 (2017).
- Da Lio, C., Teatini, P., Strozzi, T. & Tosi, L. Understanding land subsidence in salt marshes of the Venice Lagoon from SAR interferometry and ground-based investigations. *Remote Sens. Environ.* **205**, 56–70 (2018).
- Zoccarato, C. & Da Lio, C. The Holocene influence on the future evolution of the Venice Lagoon tidal marshes. *Commun. Earth Environ.* **2**, 77 (2021).
- Bomer, E. J., Wilson, C. A., Hale, R. P., Hossain, A. N. M. & Rahman, F. A. Surface elevation and sedimentation dynamics in the Ganges-Brahmaputra tidal delta plain, Bangladesh: Evidence for mangrove adaptation to human-induced tidal amplification. *Catena* **187**, 104312 (2020).
- Brain, M. J. et al. Quantifying the contribution of sediment compaction to late Holocene salt-marsh sea-level reconstructions, North Carolina, USA. *Quaternary Res.* **83**, 41–51 (2015).

28. Brain, M. J. et al. Exploring mechanisms of compaction in salt-marsh sediments using Common Era relative sea-level reconstructions. *Quat. Sci. Rev.* **167**, 96–111 (2017).
29. Törnqvist, T. E., Jankowski, K. L., Li, Y.-X. & González, J. L. Tipping points of Mississippi delta marshes due to accelerated sea-level rise. *Sci. Adv.* **6**, eaaz5512 (2020).
30. Keogh, M. E., Törnqvist, T. E., Kolker, A. S., Erkens, G. & Bridgeman, J. G. Organic matter accretion, shallow subsidence, and river delta sustainability. *J. Geophys. Res. Earth Surf.* **126**, e2021JF006231 (2021).
31. Gibson, R. E. The progress of consolidation in a clay layer increasing in thickness with time. *Geotechnique* **8**, 171–182 (1958).
32. Gambolati, G. Equation for one-dimensional vertical flow of groundwater. I. The rigorous theory. *Water Resour. Res.* **9**, 1022–1028 (1973).
33. Terzaghi, K. *From Theory to Practice in Soil Mechanics* (John Wiley & Sons Inc., 1960).
34. Santelmann, M. V., Boisjolie, B. A., Flitcroft, R. & Gomez, M. Relationships between salt marsh vegetation and surface elevation in Coos Bay Estuary, Oregon. *Northwest Sci.* **93**, 137–154 (2019).
35. McMillan, T. C., Rau, G. C., Timms, W. A. & Andersen, M. S. Utilizing the impact of earth and atmospheric tides on groundwater systems: a review reveals the future potential. *Rev. Geophys.* **57**, 281–315 (2019).
36. Bondesan, A. & Furlanetto, P. Artificial fluvial diversions in the mainland of the Lagoon of Venice during the 16th and 17th centuries inferred by historical cartography analysis. *Geomorphol. Relief, Process. Environ.* **18**, 175–200 (2012).
37. D’Alpaos, L. *Fatti e misfatti di idraulica lagunare. La laguna di Venezia dalla diversione dei fiumi alle nuove opere delle bocche di porto* (Istituto Veneto di Scienze, Lettere e Arti. Istituto Veneto di Scienze, Lettere ed Arti, Venice, 2010).
38. Tosi, L. et al. *Note Illustrative della Carta Geologica d’Italia alla scala 1:50.000. Foglio 148-149, Chioggia-Malamocco* (APAT, Dipartimento Difesa del Suolo, Servizio Geologico d’Italia. SystemCart, Roma (Italia), 2007).
39. Roner, M. et al. Detecting the delayed signatures of changing sediment supply in salt-marsh landscapes: the case of the Venice Lagoon (Italy). *Front. Mar. Sci.* **8**, 742603 (2021).
40. Allen, J. R. L. Geological impact on coastal wetland landscapes: some general effects of sediment autocompaction in the Holocene of northwest Europe. *Holocene* **9**, 1–12 (1999).
41. Long, A. J., Waller, M. P. & Stupples, P. Driving mechanisms of coastal change: peat compaction and the destruction of late Holocene coastal wetlands. *Mar. Geol.* **225**, 63–84 (2006).
42. Zoccarato, C., Törnqvist, T. E., Teatini, P. & Bridgeman, J. G. A shallow compaction model for Holocene Mississippi Delta sediments. *Proc. Int. Assoc. Hydrol. Sci.* **382**, 565–570 (2020).
43. Roner, M. et al. Spatial variation of salt-marsh organic and inorganic deposition and organic carbon accumulation: Inferences from the Venice lagoon, Italy. *Ad. Water Res.* **93**, 276–287 (2016).
44. Stralberg, D. et al. Evaluating tidal marsh sustainability in the face of sea-level rise: a hybrid modeling approach applied to San Francisco Bay. *PLoS ONE* **6**, 1–18 (2011).
45. Brain, M. J. et al. Modelling the effects of sediment compaction on salt marsh reconstructions of recent sea-level rise. *Earth Planet. Sci. Lett.* **345–348**, 180–193 (2012).
46. Schuerch, M., Rapaglia, J., Liebetrau, V., Vafeidis, A. & Reise, K. Salt marsh accretion and storm tide variation: an example from a Barrier Island in the North Sea. *Estuar. Coasts* **35**, 486–500 (2012).
47. Giao, P. H., Thoang, T. T., Thuyen, L. X. & Vu, N. H. H. Geotechnical characterization of the subsoil profile underlying the land subsidence monitoring points in Southern Vietnam Delta. *9th Int. Symp. Lowl. Technol.* **1**, 429–436 (2014).
48. Lovelock, C. E. et al. The vulnerability of Indo-Pacific mangrove forests to sea-level rise. *Nature* **526**, 559–563 (2015).
49. Hoitink, A. J. F. et al. Resilience of river deltas in the Anthropocene. *J. Geophys. Res. Earth Surf.* **125**, e2019JF005201 (2020).
50. Knappett, J. & Craig, R. *Craig’s Soil Mechanics* 9th edn (CRC Press, 2019).
51. Teatini, P., Gambolati, G., Ferronato, M., Settari, A. T. & Walters, D. Land uplift due to subsurface fluid injection. *J. Geodyn.* **51**, 1–16 (2011).
52. Biscontin, G., Cola, S., Pestana, J. M. & Simonini, P. Unified compression model for Venice Lagoon natural silts. *J. Geotech. Geoenviron. Eng.* **133**, 932–942 (2007).
53. Jamiolkowski, M., Ricceri, G. & Simonini, P. Safeguarding Venice from high tides: site characterization and geotechnical problems. In *Proceedings of 17th ICSMGE – International Conference on Soil Mechanics and Geotechnical Engineering* (ed Hamza, M.) 215–216 (IOS Press Publ, 2009).
54. Gentilomo, M. & Ceconi, G. Flood protection system designed for Venice. *Hydropower Dams* **2**, 46–52 (1997).
55. Castelletto, N., Gambolati, G. & Teatini, P. A coupled mfe poromechanical model of a large-scale load experiment at the coastland of Venice. *Comput. Geosci.* **19**, 17–29 (2015).
56. Berengo, V., Benz, T., Simonini, P. & Leoni, M. Site monitoring and numerical modelling of a trial embankment’s behaviour on Venice Lagoon soils. *ISRN Civ. Eng.* **2011**, 378579 (2011).
57. Chirol, C. et al. Effect of vegetation cover and sediment type on 3D subsurface structure and shear strength in saltmarshes. *Earth Surf. Process. Landf.* **46**, 2279–2297 (2021).
58. Mesri, G. & Castro, A. c_v/c_c concept and k_0 during secondary compression. *J. Geotechn. Eng.* **113**, 230–247 (1987).
59. Mariotti, S. F. & Kearney, W. S. Soil creep in salt marshes. *Geology* **44**, 459–462 (2016).
60. Tosi, L., Teatini, P., Bincoletto, L., Simonini, P. & Strozzi, T. Integrating geotechnical and interferometric sar measurements for secondary compressibility characterization of coastal soils. *Surv. Geophys.* **33**, 907–926 (2012).
61. Simonini, P., Ricceri, G. & Cola, S. Geotechnical characterization and properties of Venice lagoon heterogeneous silts. In *Proceedings of the 2nd International Workshop on Characterization and Properties of Natural Soils* (eds Tan, T., Phoon, K., Hight, D. & Leroueil, S.) 4, 2289–2327 (Balkema, Rotterdam, 2007).
62. ASTM D6913 Standard Test Methods for Particle-Size Distribution (Gradation) of Soils Using Sieve Analysis (ASTM, International West Conshohocken, PA).
63. ASTM D7928 Standard Test Method for Particle-Size Distribution (Gradation) of Fine-Grained Soils Using the Sedimentation (Hydrometer) Analysis (ASTM, International West Conshohocken, PA).
64. ASTM D7348 Standard Test Methods for Loss on Ignition (LOI) of Solid Combustion Residues (ASTM, International West Conshohocken, PA).
65. Zoccarato, C. Loading Experiment Database – Venice Lagoon (Italy) [Data set]. Centro di Ateneo per le Biblioteche dell’Università degli Studi di Padova (accessed 29 September 2022); <https://doi.org/10.25430/RESEARCHDATA.CAB.UNIPD.IT.00000715> (2022).
66. Brooks, H. et al. How strong are salt marshes? Geotechnical properties of coastal wetland soils. *Earth Surf. Process. Landf.* **47**, 1390–1408 (2022).
67. Cola, S., Sanavia, L., Simonini, P. & Schrefler, B. A. Coupled thermohydronechanical analysis of Venice lagoon salt marshes. *Water Resour. Res.* **44**, 1–16 (2008).
68. Toan, D. M. & Nu, N. T. Studying on the engineering geological characteristics of Middle-Upper Holocene formation (in Vietnamese, English summary). *Tap Chi GIA CHAT, Loat A* **333**, 47–56 (2013).
69. Hoang, T. M., van Lap, N., Oanh, T. T. K. & Jiro, T. The influence of delta formation mechanism on geotechnical property sequence of the late Pleistocene-Holocene sediments in the Mekong River Delta. *Heliyon* **2**, e00165 (2016).
70. Kemp, A. C. et al. Relative sea-level change in Newfoundland, Canada during the past ~3000 years. *Quaternary Sci. Rev.* **201**, 89–110 (2018).
71. van Asselen, S., Karssenberg, D. & Stouthamer, E. Contribution of peat compaction to relative sea-level rise within Holocene deltas. *Geophys. Res. Lett.* **38**, L24401 (2011).
72. van Asselen, S. The contribution of peat compaction to total basin subsidence: implications for the provision of accommodation space in organic-rich deltas. *Basin Res.* **23**, 239–255 (2011).

Acknowledgements

We thank Giuseppe Zambon (CNR, Venice – Retired) who carried out the leveling surveys at Lazzaretto Nuovo marsh in 2019. We also would like to acknowledge the great assistance in the field provided by Stefano Pasquali (CNR, Venice) and the crew of the research boat Litus (CNR) Daniele Penzo, Mauro Penzo, and Gianni Zennaro. This research was supported by VENEZIA-2021 Research Programme, Topic 3.1, funded by the “Provveditorato Interregionale Opere Pubbliche per il Veneto, Trentino Alto Adige e Friuli Venezia Giulia” through the “Concessionario Consorzio Venezia Nuova” and coordinated by CORILA, Venice. The research was also supported by Fondazione CARIPARO through the proposal HIETE (The Holocene Imprint on the future Evolution of Transitional Environments). The contribution of PM was funded by the EU Marie Curie MSCA fellow “InSPIRED – Improving Subsidence PREdictions in Delta systems”.

Author contributions

C.Z., P.Z., L.T., A.B., V.G., P.S., and P.T. conceived the study. All authors carried out field work. P.Z., V.G., C.C., M.C., and S.D. carried out lab analyses. C.Z., P.S.J.M., V.G., P.S., C.C., M.C., C.D.L., and P.T. contributed to data analysis. C.Z., C.D.L., and P.T. prepare the initial draft with contribution inputs from V.G., C.C., P.S.J.M., and M.C. All authors reviewed and edited the manuscript.

Competing interests

The authors declare no competing interests. C.Z. is an Editorial Board Member for Communications Earth & Environment, but was not involved in the editorial review of, nor the decision to publish this article.

Additional information

Supplementary information The online version contains supplementary material available at <https://doi.org/10.1038/s43247-022-00600-9>.

Correspondence and requests for materials should be addressed to Pietro Teatini.

Peer review information *Communications Earth & Environment* thanks Javier Lloret, Zhen-Ming Ge and Geoff Richards for their contribution to the peer review of this work. Primary Handling Editors: Adam Switzer, Joe Aslin, Heike Langenberg. Peer reviewer reports are available.

Reprints and permission information is available at <http://www.nature.com/reprints>

Publisher's note Springer Nature remains neutral with regard to jurisdictional claims in published maps and institutional affiliations.



Open Access This article is licensed under a Creative Commons Attribution 4.0 International License, which permits use, sharing, adaptation, distribution and reproduction in any medium or format, as long as you give appropriate credit to the original author(s) and the source, provide a link to the Creative Commons license, and indicate if changes were made. The images or other third party material in this article are included in the article's Creative Commons license, unless indicated otherwise in a credit line to the material. If material is not included in the article's Creative Commons license and your intended use is not permitted by statutory regulation or exceeds the permitted use, you will need to obtain permission directly from the copyright holder. To view a copy of this license, visit <http://creativecommons.org/licenses/by/4.0/>.

© The Author(s) 2022